SCIEPublish

Article

Visible Monuments above and below Ground Level, a Time-Honored Site from the Late Bronze Age to Modern Times

Dimitris Kaimaris *

School of Spatial Planning and Development, Aristotle University of Thessaloniki, 54124 Thessaloniki, Greece

* Corresponding author. E-mail: kaimaris@auth.gr (D.K.)

Received: 30 November 2024; Accepted: 16 January 2025; Available online: 20 January 2025

ABSTRACT: Due to the complex geometry of the monuments, it is often necessary to adapt the image collection process for their mapping. For the optimal mapping of the stronghold of Lazaritsa Chorygi (Greece) and its slopes, vertical, inclined, and horizontal images from different heights were collected using an Unmanned Aircraft System. Thus, for a monument of special archaeological/historical interest and natural beauty, a large set of high-spatial resolution data and final products (digital surface model and orthophotomosaic with spatial resolution 5.6 cm and 2.8 cm, respectively) is available. In addition, in the wider area of the fortified site, military structures (fire trenches, communication trenches, shelters, front and support trenches, and strong points) of the Great War length of 9 km were identified and mapped, which were identified in the 2003 or 2004 Google Earth Pro images, but worryingly are almost absent from the contemporary Google Earth Pro images.

Keywords: Unmanned Aerial System; Stronghold; Military structures; Complex geometry; Collecting images; Digital surface model; Orthophoto mosaic; Spatial resolution

1. Introduction

In the plain of Kilkis prefecture (Greece), 44 km north of the city of Thessaloniki (Figure 1), rises the stronghold of Lazaritsa Chorygi (41°0′52.45″ N 22°42′29.59″ E, Figure 2). It is visible from tens of kilometers away and is the result of a natural geological formation of bedrock. In prehistoric and historical times, the hill served as the citadel of the settlement that stretched along its slopes. It was of particular strategic importance from antiquity to Byzantine and modern times. The archaeological research findings date from the Late Bronze Age to the Middle Byzantine period. Fragments of pottery, mainly from the Classical period, have been found, while a bronze helmet from the 4th century BC with an engraved representation of lions on its front has been found after the desecration of a grave. An important find is a small statue of the goddess Aphrodite, dating from the late Hellenistic period. Also, a very important fact is that the settlement has not been linked to an ancient site. The current "ravaged" form of the hill's slopes is the result of the 1985 operation to create land steps for its reforestation, which destroyed the antiquities [1,2].

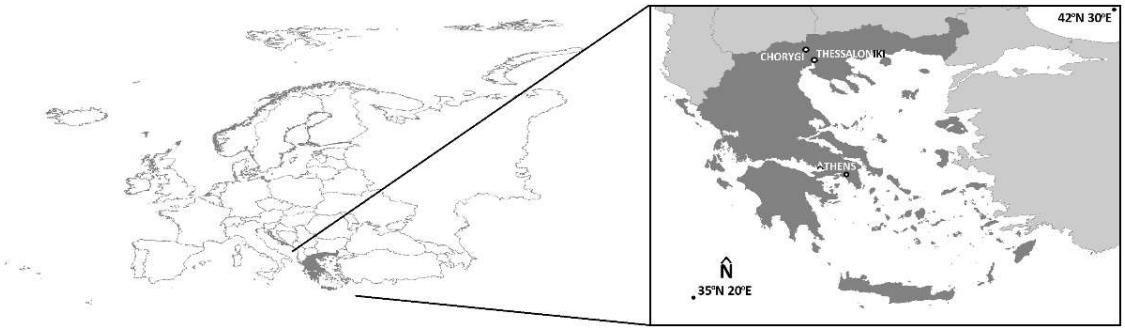

Figure 1. The location of Greece in Europe and the locations of the archaeological sites of the Lazaritsa Chorygi in Greece.

https://doi.org/10.70322/dav.2025.10003

Figure 2. The stronghold of Lazaritsa Chorygi (**left** figure approaching from southwest, **right** figure approaching from southeast).

The first objective of this paper is the creation of a Digital Surface Model (DSM) and Orthophotomosaic of the stronghold of Lazaritsa Chorygi, as this area of great archaeological/historical interest and special natural beauty has not yet been mapped.

During the First World War (1914–1918) and after the arrival of the armies of the East in 1915, the hill was fortified by French soldiers, who must have built military trenches near the hill and in the surrounding area. After the French moved further west, English soldiers [1] settled on the hill. Close observation of the hill and the surrounding area using Google Earth Pro (GEP) images led to the discovery of military trenches located a short distance to the northwest, north, and northeast of the hill. This was carried out in the older GEP images, as in the most recent images, the structures are mostly covered by crops or soil.

Thus, another aim of this paper is to map these military trenches, which are almost absent from modern GEP images.

2. Methods, Processing and Products

2.1. Unmanned Aircraft System and Google Erath Pro

The Unmanned Aircraft System (UAS) used in this work was the DJI Mini 3 Pro, which has a 48 MegaPixels (MP) RGB 1/1.3″ CMOS sensor [3]. The manual image trigger allows the collection of images with a resolution of 48 MP. However, in the shots that were taken, the trigger was automatically activated (e.g., using timelapse), resulting in a 12 MP resolution for all images.

Google Earth Pro (GEP) is an open-source software with time-lapse images collected by satellite or airborne sensors, used by both the public and scientists in a variety of applications (mapping forest areas, urban areas, *etc.*) [4–9] and policymakers, *etc.* [10,11]. GEP images are only RGB composites (lacking universal Multispectral-MS images); therefore true DNs of the original images cannot be retrieved. Nevertheless, they allow for visual data collection and exploration, such as mapping, monitoring, and managing existing archaeological sites and landscapes, as well as the identification of marks of new archaeological remains beneath the soil [12–25]. Survey areas can be anywhere in the world, and their extent is not subject to constraints, thus facilitating studies that conduct research at any scale. For the paper, GEP images from 2004 were utilized as military trenches are almost absent in modern images.

2.2. Flight Plans and Image Collection

A vertical collection of images would not allow a complete mapping of the hill, as the bedrock also creates surfaces that either develop vertically or are indented. Therefore, an additional collection of inclined and horizontal images were required (Figure 3).

Figure 3. The various flight heights for vertical, inclined and horizontal image collection (perspective from the west).

The three flights (vertical, inclined και horizontal capture, Table 1) with the RGB sensor of the archaeological site of Lazaritsa Chorygi took place on 23/9/2024 from 11:30 a.m.–14:00 p.m. The wind speed was 1.5 m/s (1 Beaufort) and the air temperature was 22 °C.

In the first flight (Table 1), the image capture was vertical (~90°) with 70% side and front overlap images (Figure 4). A total of 9 strips were implemented and the flight height was 40 m, steadily above the highest point (275 m) of the hill, *i.e.*, 315 m (Figure 3) above sea level (it was chosen that the UAS should not follow the terrain during image collection, as the altitude at a horizontal distance of 200 m varies up to 75 m). The distances of the objects from the sensor varied from 40 m to 115 m (due to the uneven relief), the total flight time was 10 min, and a total of 99 RGB images were collected.

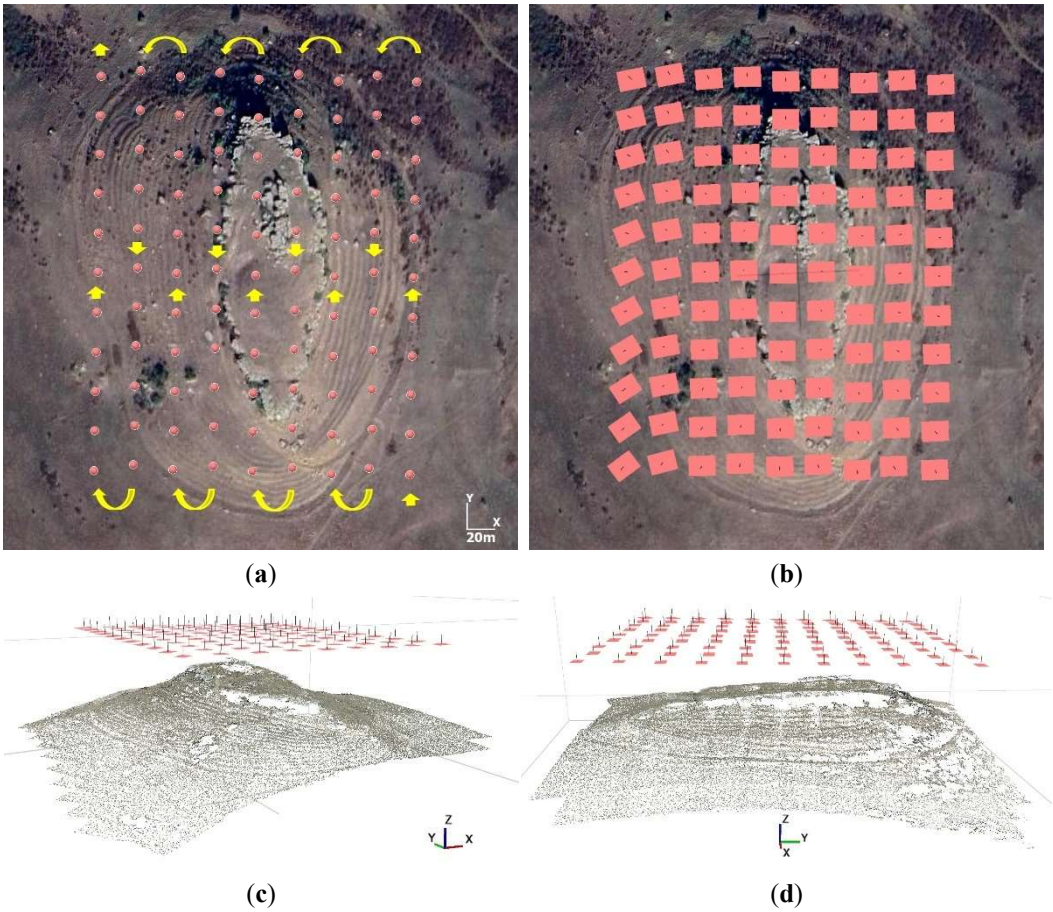

Figure 4. (**a**) Flight diagram with the positions of the capture points (Maps Data: Google Maps, image ©2024 Airbus, Maxar Technologies, Center of figure: 41°0′52.45″ N 22°42′29.59″ E). Start of image captures from the southeastern corner with a flight direction from south to north; (**b**) the layout of the vertical images and; the 3D perspectives of the collected images (**c**) from the southwest and (**d**) from the east.

Table 1. UAS data collection.

Flight	Image Collection	Overlap Images	Strips	Flight Height above Sea Level (m)	RGB Images
First	Vertical (~90º)	70% side and front	9	315	99
Second	With inclination (~45º)	70% side and front	14	315	56
Third	Horizontally (~0º)	90%	-	260 (one flight), 275 (two flights)	220

In the second flight (Table 1) the images were captured at an inclination (~45°) with 70% side and front overlap images (Figures 5 and 6). A total of 14 strips (9 strips parallel to the X-axis, Figure 5, and 5 strips parallel to the Y-axis, Figure 6) were implemented, and the flight height was again, consistently, 315 m (Figure 3) above sea level. The distances of the objects from the sensor ranged from 55 m to 145 m (due to the uneven relief), the total flight time was 16 min, and a total of 56 RGB images were collected.

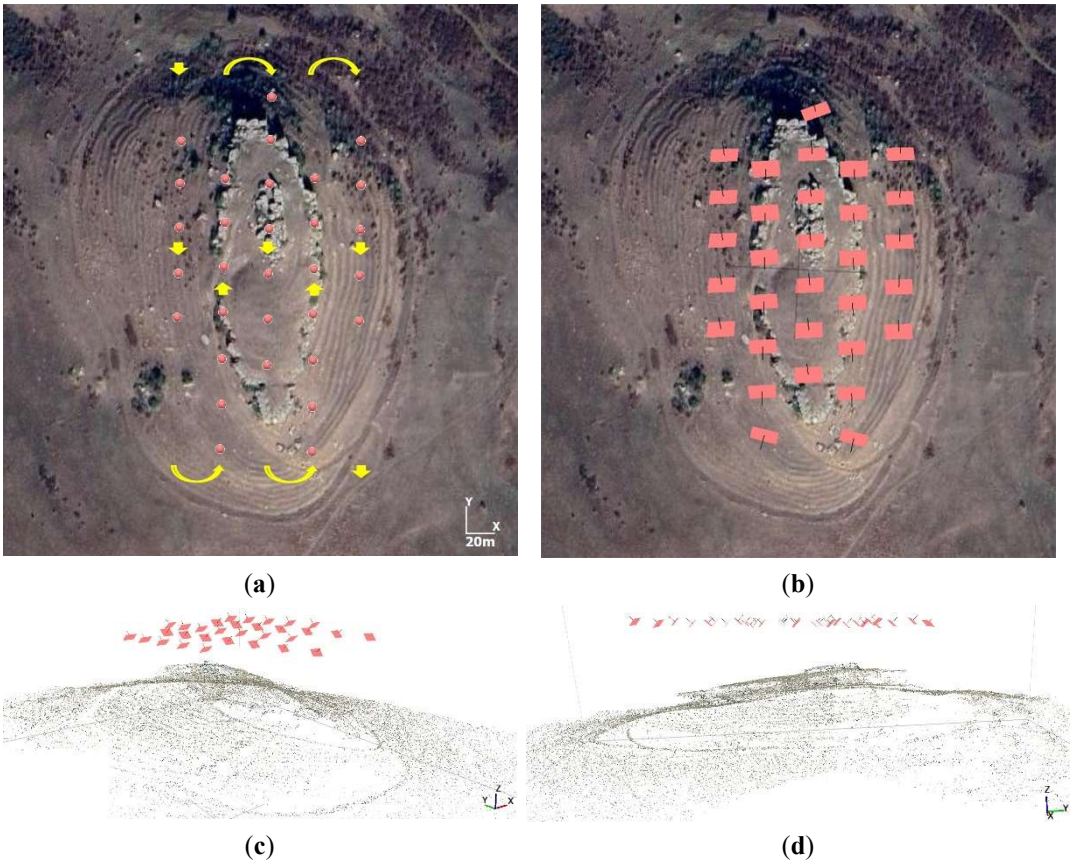

Figure 5. (**a**) Flight plan parallel to the Y-axis with the positions of the capture points (Maps Data: Google Maps, image ©2024 Airbus, Maxar Technologies, Center of figure: 41°0′52.45″ N 22°42′29.59″ E). Start of image captures from the northwestern corner with a flight direction from north to south; (**b**) the layout of the collected inclined images and; the 3D perspectives of the collected images; (**c**) from the southwest and (**d**) from the east.

Finally, in the third flight (Table 1), the image capture was performed horizontally (~0°) with ~90% overlap images. Here, three independent shorter flights were conducted. The hill does not have a circular plan view;therefore, an automatic circular flight centered on the center of the hill could not be performed so that the flight path would be uniform and the distance to the monument would be constant. In contrast, the hill has an ellipsoidal plan view, and therefore, manual flights should be performed (hence, the distances from the monument are not constant). In the first flight, the overall study object (hill slopes and bedrock) was captured, the flight height was 275 m (Figure 3) consistently above the sea surface, and the distances of the objects from the sensor ranged from 40 m to 50 m (Figure 7). In the second flight, only the bedrock was captured, the flight height was 260 m (Figure 3) consistently above the sea surface, and the distances of the objects from the sensor ranged from 25 m to 35 m (Figure 8). In the third flight, only the hilltop was captured. The flight height was 275 m (Figure 3) consistently above the sea surface and the distances of the objects from the sensor ranged from 5 m to 15 m (Figure 9). The total flight time for all three flights was 18 min, and a total of 220 RGB images were collected.

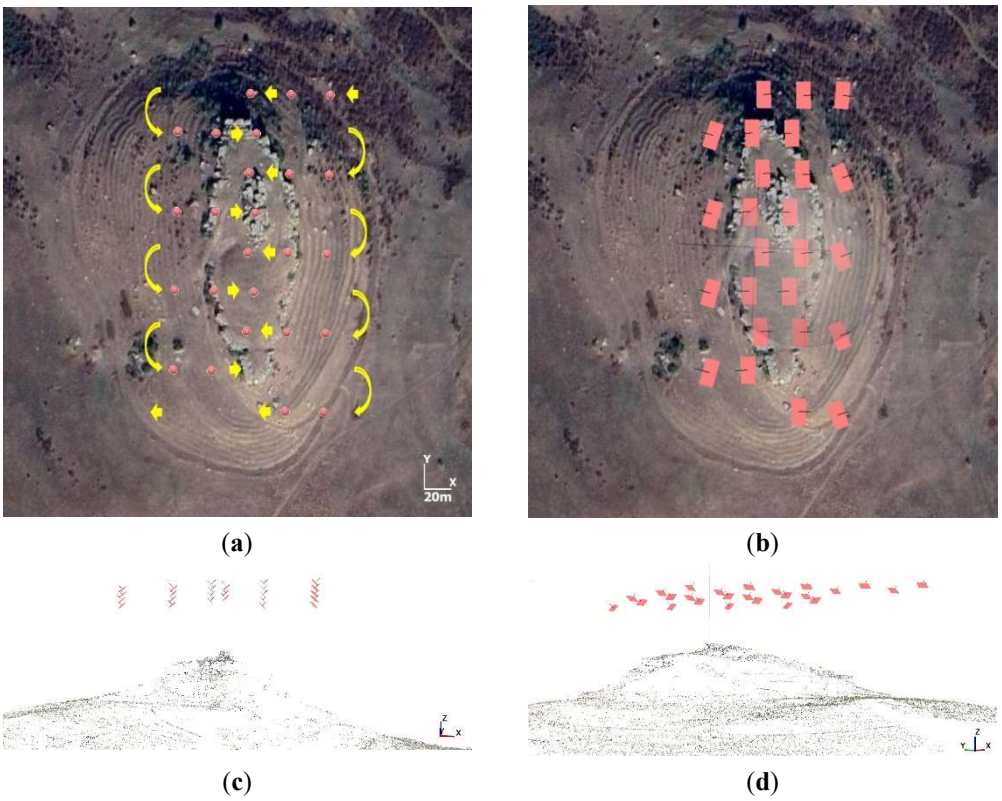

(**a**) (**b**)

(**c**) (**d**)

Figure 6. (**a**) Flight plan parallel to the X-axis with the positions of the capture points (Maps Data: Google Maps, image ©2024 Airbus, Maxar Technologies, Center of figure: 41°0′52.45″ N 22°42′29.59″ E). Start of image captures from the northeastern corner with a flight direction from east to west; (**b**) the layout of the collected inclined images and; the 3D perspectives of the collected images; (**c**) from the south and (**d**) from the southwest.

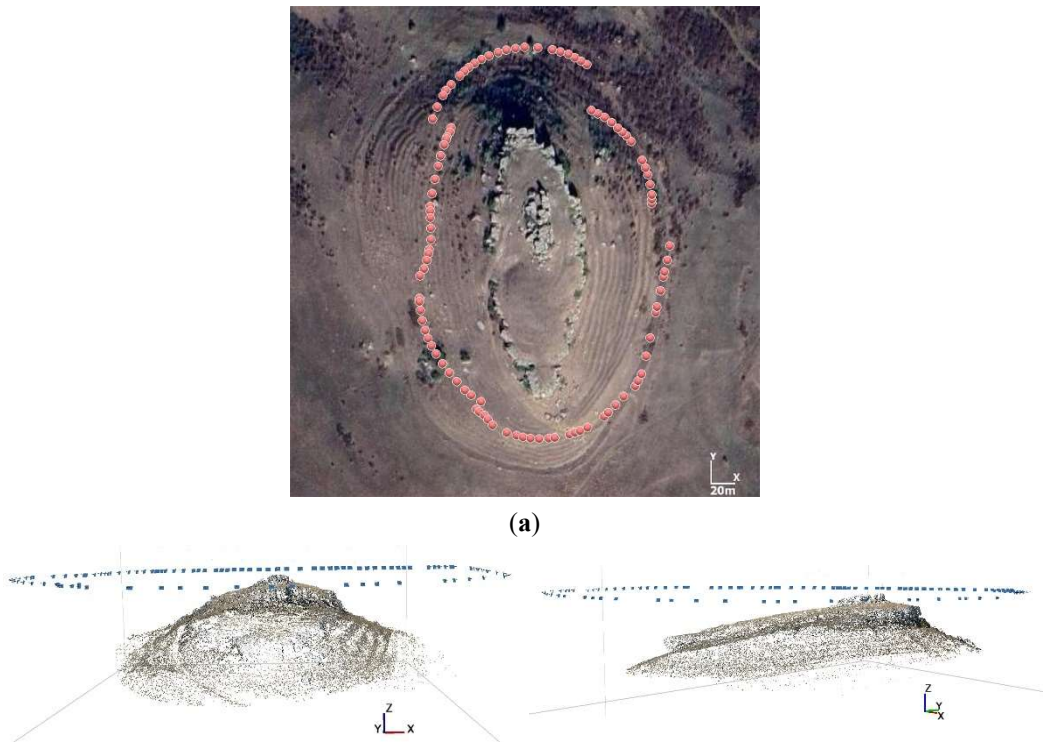

(**a**)

(**b**) (**c**)

Figure 7. First horizontal image collection flight; (**a**) the positions of the acquisition points (Map Data: Google Maps, image ©2024 Airbus, Maxar Technologies, Center of figure: 41°0′52.45″ N 22°42′29.59″ E) and; the 3D perspectives of the collected images; (**b**) from the south and (**c**) from the southeast.

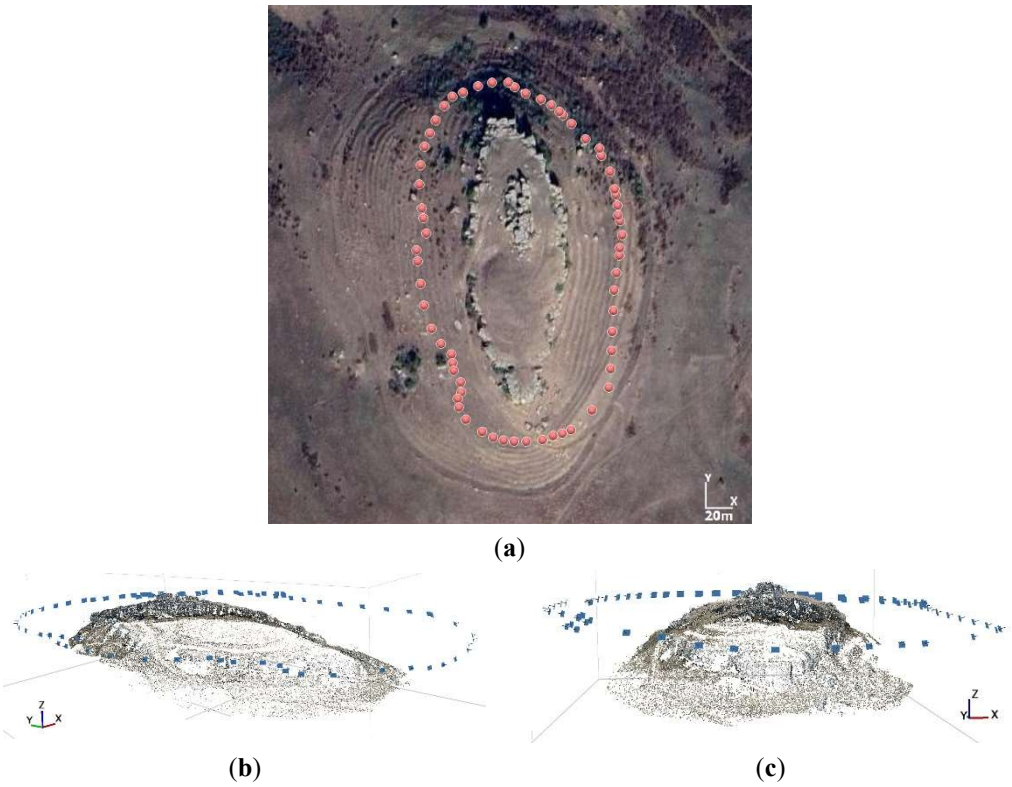

(**a**)

(**b**) (**c**)

Figure 8. Second horizontal image collection flight; (**a**) the positions of the acquisition points (Map Data: Google Maps, image ©2024 Airbus, Maxar Technologies, Center of figure: 41°0′52.45″ N 22°42′29.59″ E) and; the 3D perspectives of the collected images; (**b**) from the southwest and (**c**) from the south.

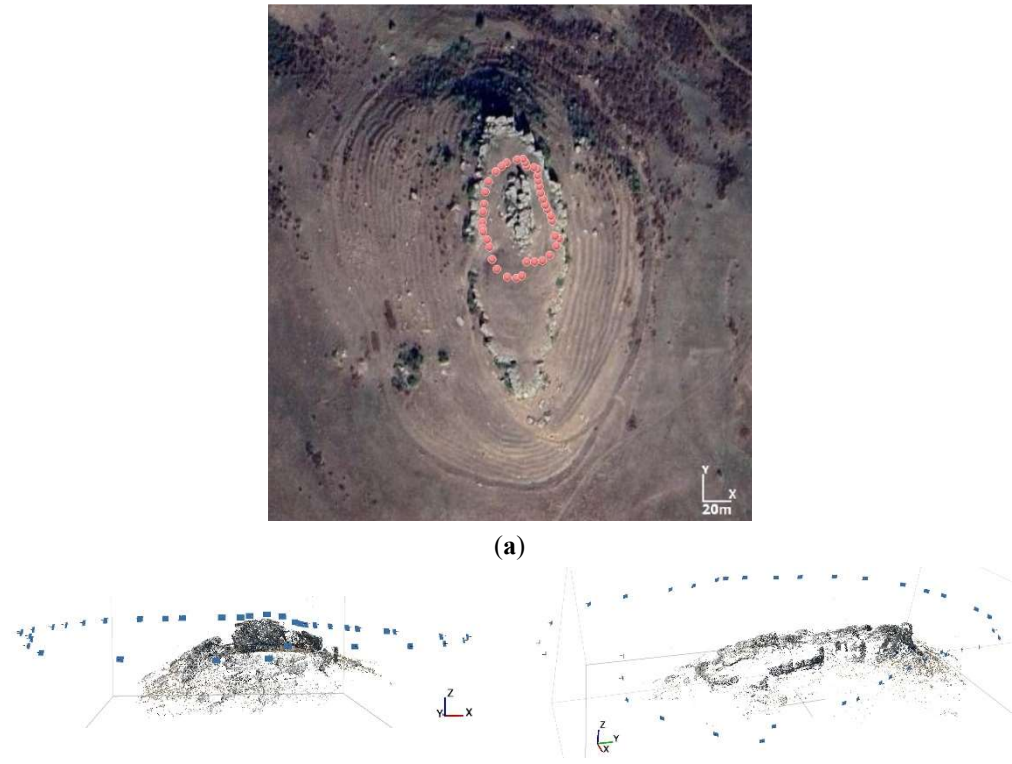

(**a**)

(**b**) (**c**)

Figure 9. Third horizontal image collection flight; (**a**) the positions of the acquisition points (Map Data: Google Maps, image ©2024 Airbus, Maxar Technologies, Center of figure: 41°0′52.45″ N 22°42′29.59″ E) and; the 3D perspectives of the collected images; (**b**) from the south and (**c**) from the southeast.

From the above paragraphs, it is evident that image collection from different flight altitudes and various capture angles can collectively ensure comprehensive photographic documentation of the monument. The determination of the model's spatial resolution and accuracy, as well as the completeness of its thematic information, remains pending.

2.3. Image Processing and Product Production

All images were imported into the Agisoft Metashape Professional© version 2.0.3 software (Figure 10). The UAS has, among others, a Global Navigation Satellite System (GNSS) (compatible with GPS, Galileo, and BeiDou), which allows the recording of the coordinates (X, Y and Z) of the center of each image collected during the flight, with an accuracy of about 3 to 5 m. The coordinates were automatically converted from World Geodetic System 1984 (WGS84) to Greek Geodetic Reference System 1987 (GGRS87) in the Agisoft Metashape Professional© version 2.0.3 software, the aligning of images (align photos with high accuracy) was performed and at the same time a sparse point cloud model based on matching pixel groups between images was generated. Meanwhile, the Root Mean Square Error for X, Y and Z coordinates ($RMSE_{XYZ}$) for all the sensor locations was calculated [26]. Then, the dense point cloud was created (build the dense cloud with high-quality and aggressive depth filtering). Next, the 3D mesh generation (build mesh) followed, where the point cloud was transformed into an actual 3D surface. The following step was conducted to build the texture (build texture), *i.e.*, the colored overlay of the generated 3D mesh. The last step was to generate a DSM and orthophotomosaic. In summary, $RMSE_{XYZ}$ is 2.42 m, 67,846,306 points (Point Cloud), 6,924,069 faces (3D Model), a DSM with spatial resolution of 5.6 cm and an orthophotomosaic with a spatial resolution of 2.8 cm were created (Figure 11).

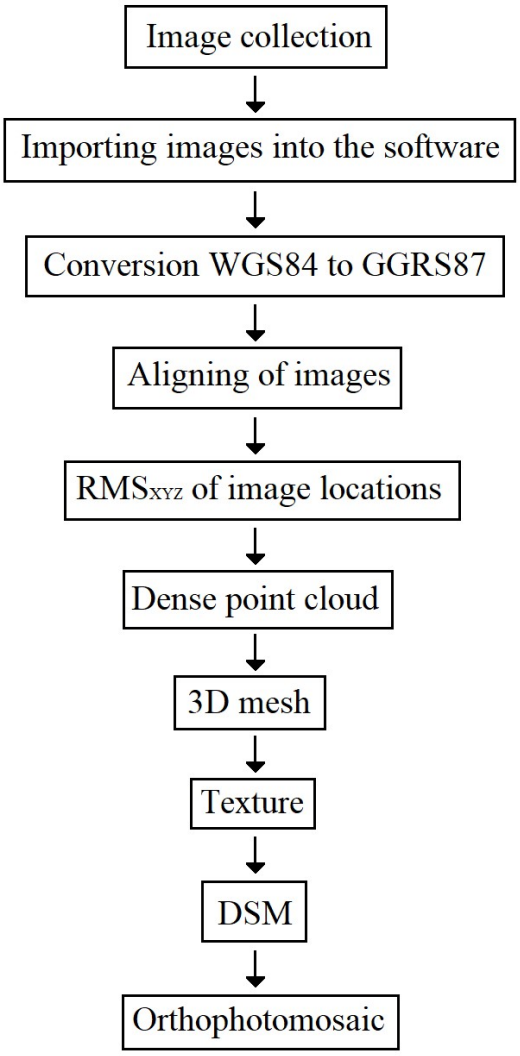

Figure 10. Workflow diagram for image processing using Agisoft Metashape Professional© version 2.0.3 software.

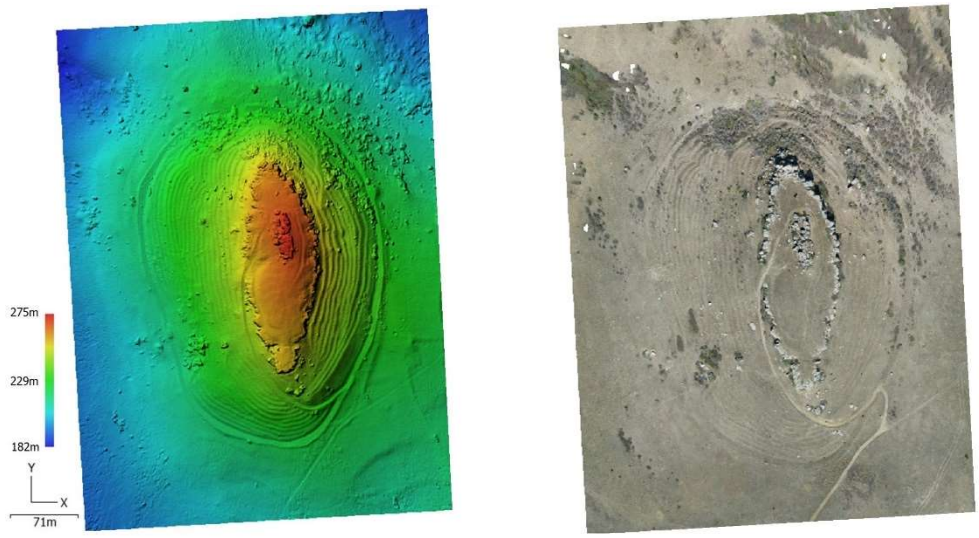

(**a**) (**b**)

Figure 11. (**a**) DSM and (**b**) orthophotomosaic (center of figures: 41°0′52.45″N 22°42′29.59″E).

2.4. Google Earth Pro

After collecting images using the UAS, the longitudinal Google Earth Pro© (GEP) version 7.1.8. 3036 images were studied for both the hill and the wider area. The visual observation of the northwest, north and northeast of the hill led to the identification in the oldest temporal images of the GEP (images for the years 2003 or 2004) of obvious remains of military trenches, which are now either completely absent or have been mostly covered by crops or soil (Figure 12). There are no crop or soil marks in the contemporary images that would indicate the presence of covered structures. However, it is hypothesized that such structures may exist beneath the crops or soil.

(**a**)

(**b**)

Figure 12. The location of military trenches in the GEP image; (**a**) of 2003 (Map Data: Google Earth, image Landsat/Copernicus, image ©2024, Maxar Technologies) and; (**b**) of 2023 (Map Data: Google Maps, image Landsat/Copernicus, image ©2024, Airbus). The almost total absence of structures is evident in the most recent image.

Initially, for the years 2003 or 2004, images of parts of the wider area were collected with a resolution of 8192 × 4771 pixels and at a suitable viewing scale that allows the collection of the spatial resolution available in GEP (from 0.5 to 1 m for the study area) of the images [20]. A mosaic of all the images was then created and finally, the geometric correction (1st degree polynomial transformation) of the mosaic in GGRS87 was performed, utilizing the X and Y coordinates of the reference points (20 points were used in total) retrieved from the National Cadastre website [27] (coordinate accuracy of about 1 m). The geometrically corrected mosaic has a final planimetric accuracy of 1.5 m. All processing operations described in this section were performed using Erdas Imagine 2015© version 15 software.

3. Results

According to the above paragraphs of the image processing in Agisoft Metashape Professional© version 2.0.3, the hill slopes and the bedrock were mapped using 68 million points spaced approximately 5.5 cm apart. In addition, 7 million faces were created that fully capture the geometry of the objects with exceptional texture. At the same time, it is found that all vertical surfaces and recesses were captured (Figure 13). Therefore, while the $RMSE_{XYZ}$ is 2.42 m (which is acceptable at first), the bedrock and hill slopes were captured with high spatial resolution and completeness.

Figure 14a shows the wider area to the northeast, north and northwest of the hill. Figure 14b shows the relief of the study area (source: National Cadastre, Digital Terrain Model with spatial resolution 5 m), featuring the military trenches. They have a total length of 9 km.

(**a**)

(**b**)

(**c**)

(**d**)

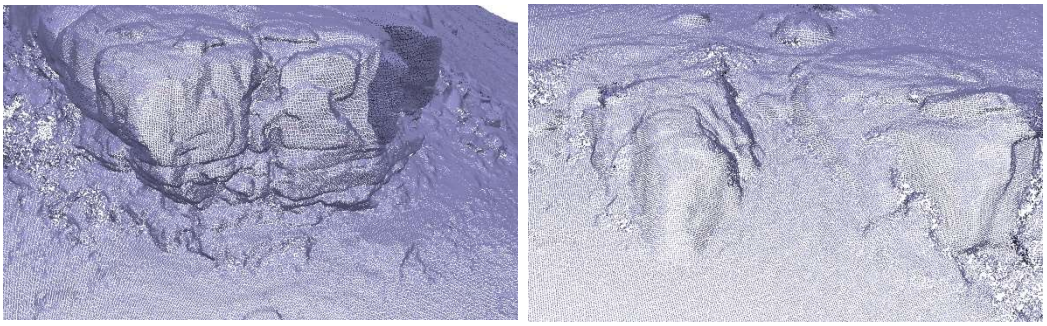

(**e**)

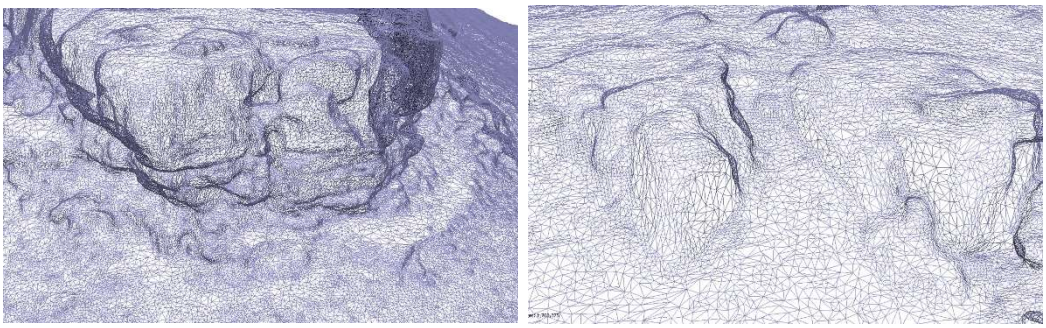

(**f**)

(**g**)

Figure 13. (**a**–**d**) 3D models of the hill and their indicative figures with (**e**) Points; (**f**) Mesh; (**g**) Textures.

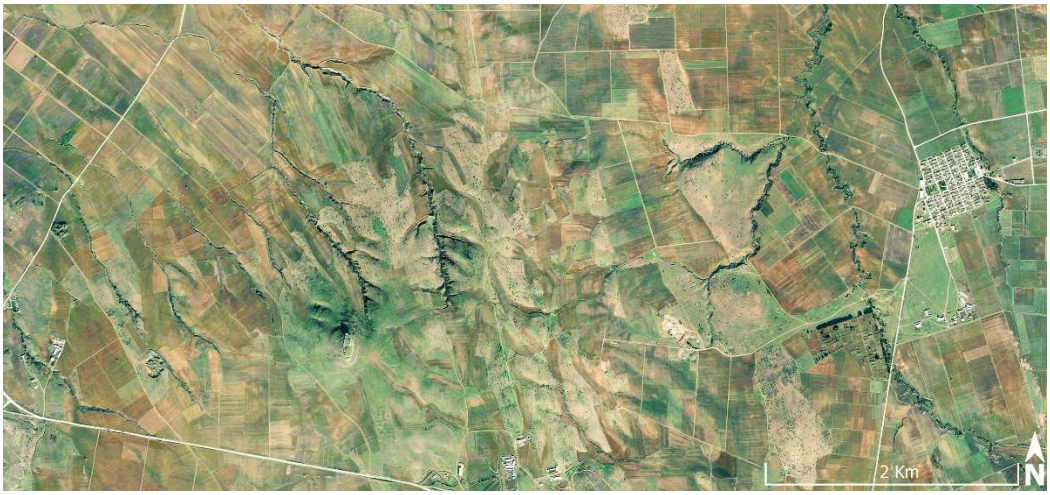

(**a**)

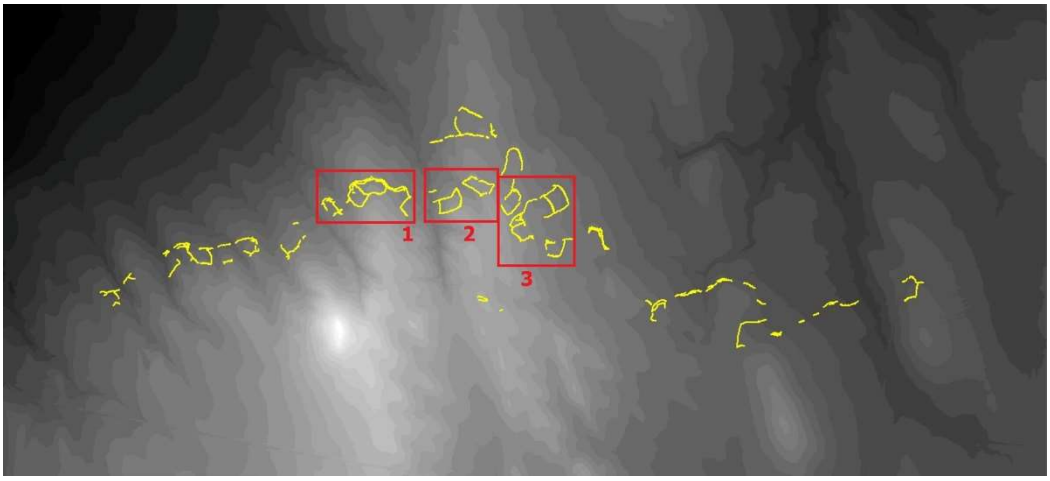

(**b**)

Figure 14. (**a**) The location of the military trenches. Southwest of the center of the figure is the location of Lazaritsa Chorygi (Map Data: Google Earth, image Landsat/Copernicus, image ©2003, Maxar Technologies); (**b**) The relief of the terrain in the study area

(light tone of grey at high altitudes to dark tone of grey at lower altitudes), and the design (in yellow) of the military trenches. In the red frame, the areas of the military trenches are presented in the following figures. Center of figures: 41°1′19.80″ N 22°43′33.77″ E.

4. Discussion

In this paper, Ground Control Points (GCPs) were not measured in the field or used during digital image processing to produce DSM and orthophotomosaic. This will be carried out in the next stage of the study (GCPs measurements, not new image acquisitions as follows), ultimately producing the above products with high spatial accuracy [28]. This study will also include the use of Lidar in UAS [29–36] to optimally capture the military graves covered by the crops and determine their degree of preservation. Thus, it is important to determine both the completeness of the monument's mapping images and whether the mapping was done with high spatial resolution (Figure 13), as well as whether the results meet a reasonably acceptable level of spatial accuracy.

In addition to the fact that the bedrock and hill slopes were captured with high spatial resolution and completeness (mapped using 68 million points, spaced approximately 5.5 cm apart, and 7 million faces created to capture the geometry of the objects with exceptional texture fully), it was found that all vertical surfaces and recesses were recorded. As a result, while high resolution orthophotomosaics can be generated, it is also possible, using the 3D model, to identify areas in the bedrock that may be at risk of rockfalls in the future (and propose preventive structural reinforcements). Military trenches act as a barrier against invasions from the north (the direction of invasion is derived from the relief of the area, Figure 14). Figures 15–17 show, by way of illustration, the positions 1–3 of Figure 14b. The types of military structure typology [29–32,37–40] observed are (e.g., Figure 15b) fire trenches, communication trenches, shelters, front and support trenches, and strong points.

More specifically, in Figure 15, we observe that the structures follow the relief of the terrain (light grey tones at higher altitudes transitioning to dark grey tones at lower altitudes, with a contour interval of 7.5 m). On the front line are the fire trenches. Parallel and at a short distance, the communication trenches are developed. At a second level and a higher altitude, the support line is observed with new fire trenches. The shelters are developed perpendicular to and between the above-mentioned fire trenches. A strong point, protected by fire trenches, is observed at one location in the southwest. In contrast, in Figure 16, no strong point is observed, but successive fire trenches (following the terrain's relief) are interconnected almost perpendicularly by communication trenches. Similar observations (as in Figure 16) are made in Figure 17, with the difference that in this area, multiple successive fire trenches are identified (four parallel fire trenches are visible). In the remaining areas of Figure 14 that are not shown, similar spatial arrangements and construction typologies are observed, with minor variations, as seen in Figures 15–17.

(**a**)

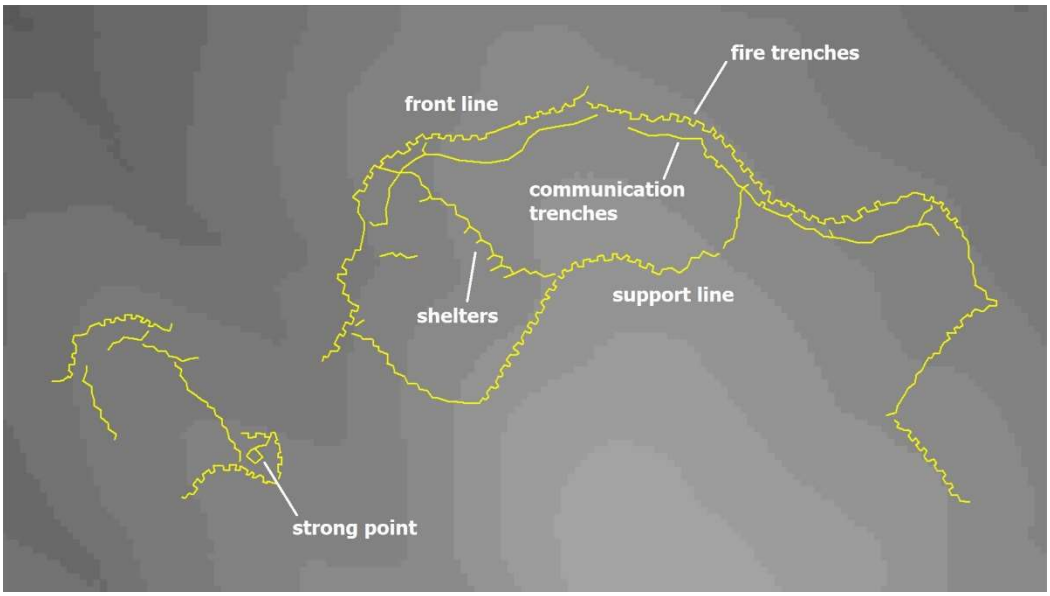

(**b**)

Figure 15. (**a**) The military trenches of position 1 of Figure 14b (Map Data: Google Earth, image Landsat/Copernicus, image ©2003, Maxar Technologies); (**b**) The relief of the terrain (light tone of grey at high altitudes to dark tone of grey at lower altitudes, the interval between contours is 7.5 m) and design (in yellow) of the military trenches. Center of figures: 41°1′27.04″ N 22°42′38.50″ E.

(**a**)

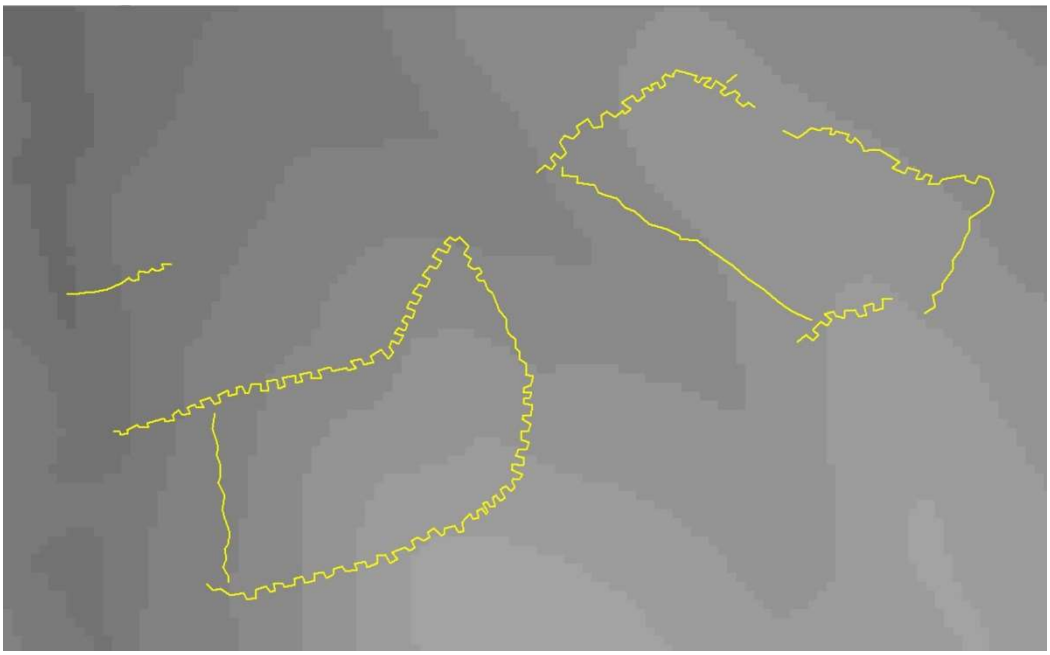

(**b**)

Figure 16. (**a**) The military trenches of position 2 of Figure 14b (Map Data: Google Earth, image Landsat/Copernicus, image ©2003, Maxar Technologies); (**b**) The relief of the terrain (light tone of grey at high altitudes to dark tone of grey at lower altitudes, the interval between contours is 7.5 m) and design (in yellow) of the military trenches. Center of figures: 41°1′27.26″ N 22°43′10.36″ E.

(**a**)

(**b**)

Figure 17. (**a**) The military trenches of position 3 of Figure 14b (Map Data: Google Earth, image Landsat/Copernicus, image ©2003, Maxar Technologies); (**b**) The relief of the terrain (light tone of grey at high altitudes to dark tone of grey at lower altitudes, the interval between contours is 7.5 m) and design (in yellow) of the military trenches. Center of figures: 41°1′21.40″ N 22°43′35.85″ E.

5. Conclusions

Due to the complex geometry of a monument, the process of collecting images for its mapping needs to be adapted. For the optimal mapping of the stronghold of Lazaritsa Chorygi (Greece) and its slopes, besides vertical images, inclined and horizontal images were collected. Thus, for a monument that had not been mapped until now, a rich data set and final products (DSM and orthophotomosaic) of high spatial resolution have become available. In the next phase, GCPs measurements will be carried out to produce DSM and orthophotomosaic of high spatial accuracy.

Unfortunately, in most countries where military structures were built during the Great War, there is no care for their preservation. These structures are being sacrificed when there is a need for housing development, construction, or agricultural exploitation. Thus, while we are aware of the problem today as we try to trace the landscape of the great battles of antiquity (e.g., the battle of Philippi in 42 BC, Greece, for the succession of the Roman Empire after the assassination of Julius Caesar [41]), future generations, less than 100 years from now, will not be able to trace the traces of the military structures of the Great War. On the other hand, France immediately after the Great War designated a Zone Rouge (Red Zone) with restrictions on building, agriculture and forestry. As a result, the surface features of the Great War are, for the most part, extremely well preserved to this day [29,33]. In the wider area of the Lazaritsa Chorygi stronghold, Great War military structures of 9 km length were identified, which can be observed in the 2003 or 2004 GEP images, but worryingly are almost universally absent from modern images. In a next phase, Lidar in UAS will be utilized to optimally capture military trenches covered by crops or natural vegetation and determine their degree of preservation. At the same time, a multispectral sensor on UAS will be used to identify the marks of the covered military structures from the soil or crop [28].

Acknowledgments

Thanks to Georgia Stratouli (Head of the Ephorate of Antiquities of Kilkis, Greece) and Nektario Poulakaki (Head of the Department of Prehistoric and Classical Antiquities and Museums of the Ephorate of Antiquities of Kilkis, Greece) for permission to collect data of the stronghold of Lazaritsa Chorygi.

Ethics Statement

Not applicable.

Informed Consent Statement

Not applicable.

Data Availability Statement

No original images or raw data will be made available on the locations, as they concern archaeological/historical sites.

Funding

This research received no external funding.

Declaration of Competing Interest

The author declares that he has no known competing financial interests or personal relationships that could have appeared to influence the work re-ported in this paper.

References

1. Chorygi—A Prominent Hill in the Plain of Kilkis with a Timeless History. Available online: http://odysseus.culture.gr/h/3/gh352.jsp?obj_id=26864 (accessed on 10 October 2024).
2. Chorygi Hill—Big Stones, Many Names, Long History. Available online: https://maxitis.gr/xristos-intos-lofos-xorugiou-megaloi-lithoi-polla-onomata-megali-istoria/ (accessed on 10 October 2024).
3. Support for DJI Mini 3 Pro. Available online: https://www.dji.com/gr/support/product/mini-3-pro (accessed on 10 October 2024).
4. Hansen MC, Potapov PV, Moore R, Hancher M, Turubanova SA, Tyukavina A, et al. High-resolution global maps of 21st-century forest cover change. *Science* **2014**, *344*, 850–853.
5. Kobayashi T, Tsend-Ayush J, Tateishi R. A New Tree Cover Percentage Map in Eurasia at 500 m Resolution Using MODIS Data. *Remote Sens.* **2014**, *6*, 209–232.
6. Carroll ML, Townshend JR, Dimiceli CM, Noojipady P, Sohlberg RA. A new global raster water mask at 250 m resolution. *Int. J. Digit. Earth* **2009**, *2*, 291–308.
7. Pekel JF, Cottam A, Gorelick N, Belward AS. High-resolution mapping of global surface water and its long-term changes. *Nature* **2016**, *540*, 418–422.
8. Schneider A, Friedl MA, Potere D. Mapping global urban areas using MODIS 500-m data: New methods and datasets based on ‘urban ecoregions’. *Remote Sens. Environ.* **2010**, *114*, 1733–1746.
9. Melchiorri M, Florczyk AJ, Freire S, Schiavina M, Pesaresi M, Kemper T. Unveiling 25 Years of Planetary Urbanization with Remote Sensing: Perspectives from the Global Human Settlement Layer. *Remote Sens.* **2018**, *10*, 768.
10. Parks L. Digging into Google Earth: An analysis of “Crisis in Darfur”. *Geoforum* **2009**, *40*, 535–545.
11. Chang M, Parrales J, Jimenez M, Sobieszczyk S, Hammer D, Copenhaver R. Kulkarni, Combining Google Earth and GIS mapping technologies in a dengue surveillance system for developing countries. *Int. J. Health Geogr.* **2009**, *8*, 1–11.
12. Myers A. Camp Delta, Google Earth and the ethics of remote sensing in archaeology. *World Archaeol.* **2010**, *42*, 455–467.
13. Myers A. Field work in the age of digital reproduction: A review of the potentials and limitations of Google Earth for archaeologists. *SAA Archaeol. Rec.* **2010**, *4*, 7–11.
14. Luo L, Wang X, Guo H, Liu C, Liu J, Li L, et al. Automated extraction of the archaeological tops of Qanat shafts from VHR Imagery in Google Earth. *Remote Sens.* **2014**, *6*, 11956–11976.
15. Pringle H. Google Earth shows clandestine worlds. *Science* **2010**, *329*, 1008–1009.
16. Palmer R. Google Maps. *AARGnews* **2005**, *31*, 38–39.
17. Beck A. Google earth and world wind: Remote sensing for the masses? *Antiquity* **2006**, *80*, 308.
18. Ur J. Google Earth and archaeology. *SAA Archaeol. Rec.* **2006**, *6*, 35–38.
19. Parcak S. *Satellite Remote Sensing for Archaeology*; Routledge Press: New York, NY, USA, 2009.
20. Kaimaris D, Georgoula O, Patias P, Stylianidis E. Comparative analysis on the archaeological content of imagery from Google Earth. *J. Cult. Herit.* **2011**, *12*, 263–269.
21. Lasaponara R, Masini N. Beyond modern landscape features: New insights in the archaeological area of Tiwanaku in Bolivia from satellite data. *Int. J. Appl. Earth Obs. Geoinf.* **2014**, *26*, 464–471.
22. Kennedy D, Bishop MC. Google earth and the archaeology of Saudi Arabia: A case study from the Jeddah area. *J. Archaeol. Sci.* **2011**, *38*, 1284–1293.
23. Thomas D, Kidd F, Nikolovski S, Zipfel C. The archaeological sites of Afghanistan in Google Earth. *AARGnews* **2008**, *37*, 22–30.
24. Sadr K, Rodier X. Google Earth, GIS and stone-walled structures in southern Gauteng, South Africa. *J. Archaeol. Sci.* **2012**, *39*, 1034–1042.

25. Brown Vega M, Craig N, Asencios Lindo G. Ground truthing of remotely identified fortifications on the central coast of Perú. *J. Archaeol. Sci.* **2013**, *38*, 1680–1689.
26. Agisoft Metashape User Manual, Professional Edition, Version 2.0. Available online: https://www.agisoft.com/pdf/metashape-pro_2_0_en.pdf (accessed on 10 October 2024).
27. Availability Search—Sales of Aerial Photos. Available online: https://gis.ktimanet.gr/gis/apr/ (accessed on 10 October 2024).
28. Kaimaris D. Aerial Remote Sensing Archaeology—A Short Review and Applications. *Land* **2024**, *13*, 997.
29. Gheyle W, Stichelbaut B, Saey T, Note N, Van den Berghe H, Van Eetvelde V, et al. Scratching the surface of war. Airborne laser scans of the Great War conflict landscape in Flanders (Belgium). *Appl. Geogr.* **2018**, *90*, 55–68.
30. Breg Valjavec M, Zorn M, Ribeiro D. Mapping War Geoheritage: Recognising Geomorphological Traces of War. *J. Open Geosci.* **2018**, *10*, 385–394.
31. de Matos-Machado R, Toumazet PJ, Bergès CJ, Amat PJ, Arnaud-Fassetta G, Bétard F, et al. War landform mapping and classification on the Verdun battlefield (France) using airborne LiDAR and multivariate analysis. *Earth Surf. Process. Landf.* **2019**, *44*, 1430–1448.
32. Zalewska A, Jakubczak M, Czarnecki J. Archaeological revival of memory of the Great War. The role of LiDAR in tracing the boundaries of the WWI Rawka Battlefield Cultural Park. *Archaeol. Pol.* **2015**, *53*, 407–412.
33. De Matos-Machado R, Amat JP, Arnaud-Fassetta G, Bétard F. Potentialités de l'outil LiDAR pour cartographier les vestiges de la Grande Guerre en milieu intra-forestier (bois des Caures, forêt domaniale de Verdun, Meuse). *EchoGéo* **2016**, *38*, 1–22.
34. Ronchi D, Limongiello M, Barba S. Correlation among Earthwork and Cropmark Anomalies within Archaeological Landscape Investigation by Using LiDAR and Multispectral Technologies from UAV. *Drones* **2020**, *4*, 72.
35. Casana J, Laugier JE, Hill CA, Reese MK, Ferwerda C, McCoy DM, et al. Exploring archaeological landscapes using drone-acquired lidar: Case studies from Hawai'i, Colorado, and New Hampshire, USA. *J. Archaeol. Sci. Rep.* **2021**, *39*, 103133.
36. Li Z. New opportunities for archaeological research in the Greater Ghingan Range, China: Application of UAV LiDAR in the archaeological survey of the Shenshan Mountain. *J. Archaeol. Sci. Rep.* **2023**, *51*, 104182.
37. Stichelbaut B, Note N, Saey T, Hanssens D, Van den Berghe H, Bourgeois J, et al. Non-invasive research of tunneling heritage in the Ypres Salient (1914–1918)—research of the Tor Top tunnel system. *J. Cult. Herit.* **2017**, *26*, 109–117.
38. Wisniewski DK, Doyle P, Hunter RJS, Pringle JK, Stimpson IG, Wright D, et al. A multidisciplinary scientific investigation of the 1916 Hawthorn Mine Crater, Beaumont Hamel, Somme, Northern France. *J. Confl.Archaeol.* **2023**, *18*, 125–156.
39. Stichelbaut B. The First Thirty Kilometresof theWestern Front 1914–1918: An Aerial Archaeological Approach with Historical Remote Sensing Data. *Archaeol. Prospect.* **2011**, *18*, 57–66.
40. Stichelbaut B, Gheyle W, Van Eetvelde V, Van Meirvenne M, Saey T, Note N, et al. The Ypres Salient 1914–1918: Historical aerial photography and the landscape of war. *Antiquity* **2017**, *91*, 235–249.
41. Georgoula O, Kaimaris D, Karadedos G, Patias P. Photogrammetry and Archaeology: A case study in the archaeological site of Philippoi in N. Greece. In Proceedings of the CAA (Computer Applications and Quantitative Methods in Archaeology) Congress, Enter the Past. The E-Way into Four Dimensions of Cultural Heritage, City Hall Vienna, Austria, 8–12 April 2003; pp. 409–413.